125Te NMR study of the bulk of topological insulators Bi2Te3 and Sb2Te3

Nachtigal, J.; Chong, S.V.; Williams, G.V.M.; Isaeva, A.; Oeckler, O.; Haase, J.; Guehne, R.

DOI
10.1002/zaac.202200208

Publication date
2022

Document Version
Final published version

Published in
Zeitschrift fur Anorganische und Allgemeine Chemie

Journal of Inorganic and General Chemistry
ZAAC
Zeitschrift für anorganische und allgemeine Chemie
www.zaac.wiley-vch.de
RESEARCH ARTICLE
DOI: 10.1002/zaac.202200208

^{125}Te NMR study of the bulk of topological insulators Bi_2Te_3 and Sb_2Te_3

Jakob Nachtigal,[a] Shen V. Chong,[b, f] Grant V. M. Williams,[c, f] Anna Isaeva,[d] Oliver Oeckler,[e] Jürgen Haase,[a] and Robin Guehne*[a]

The narrow band gap semiconductors Bi_2Te_3 and Sb_2Te_3 are well known for their room temperature thermoelectric performance. Recently, they were shown to serve as model systems of three-dimensional topological insulators with a bulk band gap and very robust, spin-resolved surface states due to a special band inversion in their periodic bulk. Evidently, it is of interest to investigate the special surface states with a local probe like nuclear magnetic resonance (NMR). However, especially the bulk NMR of these materials shows peculiar and rather unexpected phenomena, e.g., a *magnetic field* induced deformation of the local charge symmetry and excessive line broadening due to a special internuclear coupling. Here we report a comprehensive account of the room temperature NMR properties of the spin-1/2 nucleus ^{125}Te of single crystalline Bi_2Te_3 and Sb_2Te_3. This includes a very unusual spin-lattice relaxation that seems not to be reflected in the NMR shift, as well as an exchange enhanced NMR line broadening.

Introduction

The tetradymite-type compounds Bi_2Te_3 and Sb_2Te_3 have been studied for a long time due to their excellent room temperature thermoelectric performance.[1–3] In 2009, these materials and the isotypic Bi_2Se_3 were recognized as model systems of three-dimensional topological insulators with special metallic surface states that fuel expectations in the fields of quantum computing and spintronic applications.[4–6] Swiftly, nuclear magnetic resonance (NMR) as a powerful bulk probe with local resolution of electronic properties was employed with large surface-to-volume samples to detect and characterize nuclei in the proximity of the topologically protected surface states.[7–10] While an identification of nuclei near the surface has been achieved using nanopowdered samples, a characterization of the electronic surface states using NMR remains difficult. Uncertainties stem from, first, the fact that the bulk NMR of these compounds is not fully understood, although required to correctly separate the NMR signals coming from the surface.[10] Second, the electronic band structures of nanocrystalline samples can be altered as well due to quantum size effects, i.e., for very small samples, boundaries can no longer be ignored when the electronic band structure is analyzed.[11,12] In other words, it is by far not a trivial question what a sample actually represents from an electronic point of view, if the grains are reduced to nanometer dimensions.

While the above points establish NMR as a suitable probe for characterizing topological materials through their surface state properties, researchers are just at the beginning to unravel these and other properties of strongly spin-orbit coupled systems. For example, it has been shown that even the bulk NMR properties of these materials can provide crucial insight and hold fascinating phenomena. As illustrated in Figure 1, the real-space signature of the band inversion in Bi_2Se_3 (and similarly in Bi_2Te_3 and Sb_2Te_3) can be seen as a charge redistribution between different crystal sites, mainly Bi and Se_{out}. Using ^{209}Bi NMR, it is possible to sense the corresponding difference in the local charge density in quantitative agreement with DFT calculations. Here, especially doped samples are essential, because their free electrons populate the bands subject to the band inversion. This relationship is illustrated in Figure 1 with the Fermi level (E_F) and the corresponding electron locations in the chemical structure given by the dark

[a] J. Nachtigal, J. Haase, R. Guehne
Felix Bloch Institute for Solid State Physics
Leipzig University
Linnéstraße 5, 04103 Leipzig, Germany
E-mail: r.guehne@physik.uni-leipzig.de
[b] S. V. Chong
Robinson Research Institute
Victoria University of Wellington
PO Box 33436, Lower Hutt 5046, New Zealand
[c] G. V. M. Williams
School of Chemical and Physical Sciences
Victoria University of Wellington
PO Box 600, Wellington 6140, New Zealand
[d] A. Isaeva
Van der Waals-Zeeman Institute, Institute of Physics
University of Amsterdam
1098 XH Amsterdam, The Netherlands
[e] O. Oeckler
Institute for Mineralogy, Crystallography and Materials Science, Faculty of Chemistry and Mineralogy
Leipzig University
Scharnhorststr. 20, 04275 Leipzig, Germany
[f] S. V. Chong, G. V. M. Williams
The MacDiarmid Institute for Advanced Materials and Nanotechnology
SCPS, Victoria University of Wellington
PO Box 600, Wellington 6140, New Zealand

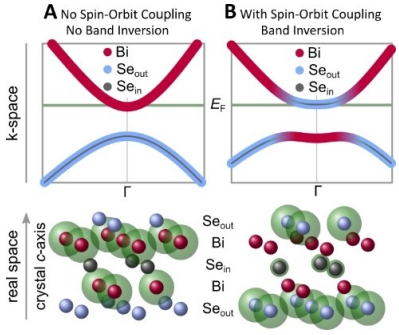

Figure 1. Sketches of the energy band gap in Bi_2Se_3 without (A) and with (B) topological band inversion induced by spin-orbit interaction. Since the band inversion alters the occupation of those bands involved - i.e. Bi bands (red) can be associated with the conduction band in the trivial case (A), while Se bands (blue and grey) form the valence band - in real space charges are re-located among the different crystal sites (dark green spheres in bottom panels). This charge re-distribution due to the band inversion can be measured quantitatively with NMR and calculated with DFT, thus providing a method to identify topological systems from their bulk properties. Note that both the crystal structure as well as the concept of band inversion apply similarly to Bi_2Te_3 and Sb_2Te_3.[4]

green spheres.[13] Hence, NMR together with DFT can be used to identify Bi_2Se_3 as a topological insulator even from its bulk properties. Another intriguing effect revealed by bulk NMR of Bi_2Se_3 and Bi_2Te_3 concerns a highly unusual magnetic field induced charge symmetry, i.e., the implication of so far unknown rotational degrees of freedom of electronic states subject to strong spin-orbit coupling (SOC) with potential consequences for other electronic properties such as heat capacity or magnetoresistance.[13–15]

Additionally, an exchange enhanced internuclear coupling (*J*-coupling) is believed not only to universally govern the behavior of each nuclear magnetic moment in the present systems, but may also be a substantial factor for magnetism in closely related compounds, such as magnetically doped Bi_2Te_3-type materials or magnetic topological insulators.[16–19] This enhanced coupling is believed to be of Bloembergen-Rowland (BR) type which is an extension of Ramsey's theory of the indirect nuclear coupling in molecules to insulating solids, and a complement to the well-known Ruderman-Kittel-Kasuya-Yosida (RKKY) interaction found in metallic solids.[20–22] As this special nuclear coupling has so far only been described with ^{77}Se NMR in Bi_2Se_3, one objective of the present manuscript is to work out evidence of such an unusually strong, indirect nuclear coupling in Bi_2Te_3 and Sb_2Te_3, as well, using magnetic field dependent ^{125}Te NMR. Furthermore, a comprehensive set of room temperature NMR parameters including inconsistent spin-lattice relaxation and shift is reported and analyzed to broaden the experimental basis required to stimulate a deeper understanding in exchange with theoretical studies, such as that reported by Boutin et al.[23]

Results and Discussion

With the crystal structure of Bi_2Te_3 and Sb_2Te_3 (space group $R\bar{3}m$) and its main building block of a quintuple layer (cf. isostructural Bi_2Se_3 in Figure 1 and details in the experimental section) comprising two *outer* Te atomic sheets (Te_{out}) two chemically equivalent pnictogen sheets (Bi/Sb), and one *inner* Te sheet (Te_{in}), one expects two ^{125}Te NMR signals for both single crystalline compounds. The relative number of nuclei occupying outer and inner lattice positions then result in a 2 to 1 signal intensity for Te_{out}: Te_{in}, that can be used to assign single crystal resonances to the two chemically and crystallografically non-equivalent crystal sites.[16,24] Note, that the two signals can be measured under identical experimental conditions if T_1 and T_2 are known, and thus, signal intensities can directly be compared.

Figure 2 shows typical ^{125}Te spectra obtained from Sb_2Te_3 (sample ST1) and Bi_2Te_3 (sample BT3) for various crystal orientations with respect to the external magnetic field B_0, where β denotes the angle between the crystal *c*-axis (crystallographic [001] direction) and B_0. For Sb_2Te_3, the two signals can only be accessed individually for angles close to $c \perp B_0$ ($\beta = 90°$). Based on their T_2-corrected relative signal intensity of 2:1, Te_{out} is identified as the dominant resonance at 515 ppm with the much broader Te_{in} shifted to 775 ppm. In case of Bi_2Te_3, the two ^{125}Te signals are well separated for most orientations, except for $\beta \approx 60°$, cf. Figure 1B. Again, their relative signal intensity allows for a clear identification as Te_{out} and Te_{in} as given in the figure. That the overlap of the two signals in both compounds is so different, i.e., that Te resonances in Bi_2Te_3 are well separated while for Te in Sb_2Te_3 the two resonances overlap essentially for all crystal orientations, already points to a peculiar shift phenomenology as discussed below. The full set of available NMR parameters for the five samples investigated within this work is summarized in Table 1.

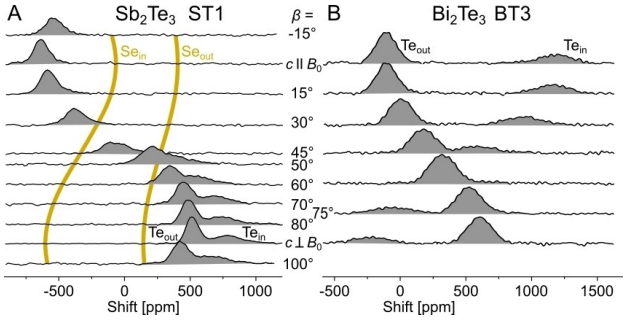

Figure 2. Spin echo ^{125}Te spectra obtained from (A) Sb_2Te_3 (ST1) and (B) Bi_2Te_3 (BT3) for various orientations (β-angle between the crystal *c*-axis and B_0), acquired at $B_0 = 11.74$ T and referenced against $(CH_3)_2Te$. The ^{125}Te resonances in both compounds show a strong dependence on the crystal orientation, as well as large, orientation independent linewidths. Also shown are the shift anisotropies of ^{77}Se resonances in Bi_2Se_3 (yellow lines) with 0 ppm corresponding to $(CH_3)_2Se$.

Table 1. Room temperature NMR properties of ^{125}Te in Bi_2Te_3 and Sb_2Te_3 for various samples obtained at 11.74 T. Isotropic (K_{iso}) and anisotropic (K_{axial}) shift contributions and spin-lattice (T_1) and spin-echo decay (T_2) times, as well as field independent (Λ_0) and dependent linewidths (b) are presented. Relaxation and line broadening data were obtained for $c \parallel B_0$ and $c \perp B_0$ for Bi_2Te_3 and Sb_2Te_3, respectively. For comparison, the Se data of Bi_2Se_3 from Georgieva et al. are shown.[16]

Sample	Label	Site	Shift		Relaxation		Line broadening		
			K_{iso} ppm	K_{axial} ppm	T_1 ms	T_2 µs	Λ_0 kHz	b kHz/T	b ppm
Sb_2Te_3	ST1	Te_{out}	145(30)	−369(23)	30(2)	400(50)		1.5(2)	112(15)
		Te_{in}	318(30)	−455(23)	20(2)	170(30)	16(4)	2.5(3)	186(22)
Sb_2Te_3	ST2	Te_{out}	178(30)	−379(30)	26(2)	414(20)		1.6(3)	119(23)
		Te_{in}	350(30)	−465(30)	19(2)	200(10)	25(4)	1.7(3)	126(22)
Bi_2Te_3	BT1	Te_{out}	375(10)	−156(20)	140(10)	125(5)	21(3)	1.4(1)	104(8)
		Te_{in}	234(15)	574(45)	310(30)	75(5)	33(3)	2.5(1)	186(8)
Bi_2Te_3	BT2	Te_{out}	398(10)	−195(20)	82(4)	120(5)	25(3)	0.4(2)	30(15)
		Te_{in}	259(15)	538(70)	151(6)	63(2)	40(3)	1.7(2)	126(15)
Bi_2Te_3	BT3	Te_{out}	437(08)	−242(08)	48(6)	150(5)	24(3)	1.5(1)	112(8)
		Te_{in}	314(10)	469(09)	62(7)	89(2)	40(3)	2.3(1)	171(8)
Bi_2Se_3		Se_{out}	233(7)	89(07)	3000	215(10)	10.9	<0.4	<50
		Se_{in}	−427(12)	181(12)	2000	95(10)	24.3	<0.4	<50

The spin-lattice relaxation has been measured for both chalcogenides and crystal sites. Due to the overlapping Te signals in Sb_2Te_3, T_1 was measured for $c \perp B_0$ yielding about 20 and 26 to 30 ms for Te_{in} and Te_{out}, respectively. In Bi_2Te_3, the spin-lattice relaxation for the three samples under investigation was measured for $c \parallel B_0$. Here, T_1 relaxation times vary substantially, between 50 and 150 ms for Te_{out} and between 60 and 300 ms for Te_{in}.

The spin-lattice relaxation for spin 1/2 ^{125}Te in Sb_2Te_3 and Bi_2Te_3 is surprisingly rapid. There are significant differences between the two different compositions, and even larger differences for Te in Bi_2Te_3. Given the high degree of self-doping known in these systems (typical Bi_2Te_3 and Sb_2Te_3 samples have carrier concentrations ranging from 10^{18} up to 10^{20}cm^{-3}due to the tendency to form native point defects, such as vacancies and antisite disorder)[25–27] fast spin-lattice relaxation hints at an interaction of the nuclear spins with those of free charge carriers. For example, T_1 of Te in Bi_2Te_3 seems to be shorter for the higher carrier concentration sample BT2 ($\sim 1.7\times10^{19}$ cm^{-3} electrons) in comparison to BT1 ($\sim 5\times10^{18}$ cm^{-3} electrons),[15] pointing to a larger Fermi level density-of-states (DOS) and suggesting BT3 to be the Bi_2Te_3 single crystal with the largest carrier concentration. Relaxation due to free carriers was also considered for ^{77}Se NMR in Bi_2Se_3, where the T_1 was reduced by about a factor of 10 due to the intercalation of Cu in $Cu_{0.15}Bi_2Se_3$, typically yielding much increased carrier concentrations.[16] But the difference in T_1 of one to two orders of magnitude for Te in Bi_2Te_3 in comparison to Se in Bi_2Se_3 (cf. Table 1) can hardly be attributed to a difference in the DOS, or simply to a larger hyperfine coupling constant for Te, as expected for a heavier element. Moreover, the finding of a spin-lattice relaxation as fast as 20 ms for Te nuclei in Sb_2Te_3 is very unusual and appears to be too short for the expected DOS, even for the typically higher carrier densities of up to 10^{20}cm^{-3} p-type carriers.[26,27] Spin-lattice relaxation in the present systems, therefore, is not easily explained and requires further investigation. It should be noted, however, that the finding may hint at a so far undocumented spin-lattice relaxation mechanism due to strongly spin-orbit coupled charge carriers as predicted with ^{209}Bi NMR in Bi_2Se_3.[13]

Next, the NMR shift anisotropy shall be addressed. From tracing the Te resonance frequencies for their changes under crystal rotation as shown exemplarily in Figure 2, the isotopic (K_{iso}) and axial (K_{axial}) shift components are readily determined and provided in Table 1 (see the experimental section for the definition of the shift components). The isotropic shifts for all Te resonances as given in Table 1 are found to be ranging between 150 and 440 ppm, depending on material, sample, and crystal site. Quite a surprising result is that while the isotropic shifts of the inner signals for Sb_2Te_3 and Bi_2Te_3 are rather similar (ranging from 234 to 350 ppm), those of the outer signals are clearly different. The absolute difference between the inner and outer isotropic shifts is about the same for both materials, but K_{iso} for Te_{out} in Sb_2Te_3 is shifted to lower and for Bi_2Te_3 to higher values. This suggests a hidden feature which might be related to differences in the material specific chemical shifts or to band structure details and the type of doping (p-type for Sb_2Te_3, n-type for Bi_2Te_3). A future study aided by first-principles calculations may yield a better understanding of this behavior as well as of the shift phenomenology in these materials in general.

Comparing the isotropic shift values to the corresponding relaxation times reveals a clear correlation, i.e., the smaller T_1, the larger the K_{iso} (cf. Table 1). This again implies a higher carrier density for BT3 in comparison to the other Bi_2Te_3 samples, as well as a higher n for ST2 compared to ST1. On the other hand, the differences in T_1 found for the same resonances are much greater than the corresponding variation of the isotropic shifts. That is, beyond a clear connection between relaxation, shift, and carrier concentration, there is no obvious model that explains the finding (given the large DOS one may assume a Fermi liquid and $T_1K_{iso}^2 = \text{const.}$). In other words, there must be field fluctuations at the Te nuclei that give rise to spin-lattice relaxation, but do not contribute to the Knight shift. In contrast,

the isotropic shifts of the two Se resonances in Bi_2Se_3 are very different, while the corresponding spin-lattice relaxation is slow and almost the same for both crystal sites (cf. Table 1) although a similar DOS as in Bi_2Te_3 can be assumed. This implies significant differences in the chemical, i.e., charge carrier independent shift for the two resonances which is perhaps more complex than in other systems due to the strong spin-orbit interaction.[23]

From the orientation dependent measurements, an axially symmetric shift anisotropy is found for each pair of resonances in the present samples (Figure 2). Axial shift symmetry is a ubiquitous feature of the bulk NMR of these types of materials, including quadrupole nuclei, in agreement with the local symmetry given by the chemical structure.[13–16]

The axial shift components are very large (e.g., more than 1500 ppm total shift range for the orientation dependence of Te_{in} in Bi_2Te_3) and show substantial variations across the samples, including different signs. For comparison, the NMR shift anisotropy of Se nuclei in single crystalline Bi_2Se_3 as taken from Georgieva et al.[16] is reproduced by the yellow lines in Figure 2 A and in Table 1. Obviously, the shift phenomenology in this family of compounds as documented in the present work is very complex. Certainly, given the large defect densities and corresponding concentrations of free carriers, charge carrier dependent shift components must be taken into account. However, in order to disentangle the various carrier independent, i.e., chemical shift contributions, from those stemming from free charge carriers, and to allow for a comparison to available theory,[23] systematic temperature dependent investigations of samples with well-defined carrier concentrations are required. Such an investigation may then also allow for a better understanding of the mechanism behind spin-lattice relaxation in the present material.

Beyond the NMR shift anisotropy, the orientation dependent spectra shown in Figure 2 reveal yet another feature of the Te NMR in Bi_2Te_3 and Sb_2Te_3, namely large and isotropic linewidths. The observed linewidths range between 15 kHz (Te_{out} in Sb_2Te_3) and more than 40 kHz (Te_{in} in Bi_2Te_3) at an external field of 11.74 T. The observation of a large and isotropic line broadening reminds one of the special internuclear coupling yielding large magnetic field *independent* linewidths of ^{77}Se resonances in Bi_2Se_3. Hence, magnetic field dependent measurements were carried out for fields from 7 to 17.6 T.

In Figure 3, typical Te spectra obtained from Bi_2Te_3 and Sb_2Te_3 single crystals for various magnetic fields are shown in units of ppm. Normally, for NMR that is governed by inhomogeneities or powder averages, typical spectra should be very similar for different external fields when plotted on the ppm scale (such as the relative frequency difference of two resonances within the same sample). This is fairly the case for Te spectra in Sb_2Te_3 where the overall lineshape of the $c \perp B_0$ spectra match almost perfectly for the different fields (Figure 3A). Te resonances in Bi_2Te_3, however, behave distinctly different. The lines are much broadened at lower fields proving substantial magnetic field independent linewidth contributions (Figure 3B).

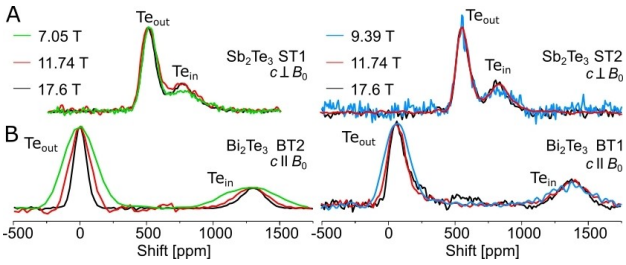

Figure 3. ^{125}Te spectra obtained from various Sb_2Te_3 (A) and Bi_2Te_3 (B) samples and external magnetic fields in units of ppm. The Te resonances in both types of samples behave quite differently, with a line broadening proportional to B_0 for Sb_2Te_3, and large magnetic field independent linewidths for Bi_2Te_3.

In Figure 4, the full width at half maximum (FWHM) of each resonance is plotted against B_0. Furthermore, a $\left(\Lambda(B_0) = \sqrt{\Lambda_0^2 + (bB_0)^2}\right)$-relation yielding the solid lines was applied to differentiate between magnetic field independent (Λ_0) and magnetic field dependent (bB_0) linewidth contributions. Obviously, Te linewidths in Bi_2Te_3 are by a factor of 1.5 (Te_{in}) to ~2 (Te_{out}) larger than those for Sb_2Te_3. Moreover, in all samples Te_{in} line broadening exceeds that of Te_{out}, in agreement with observations for Se_{in} and Se_{out} in Bi_2Se_3.[16] Most of the resonances also show a field independent linewidth of at least 20 kHz (cf. Table 1). Exclusively for Te_{out} in Sb_2Te_3, the linewidths can be very well accounted for by a $(\Lambda(B_0) = bB_0)$-relation (dashed lines in Figure 4A). As indicated by the red bars in Figure 4, direct dipole-dipole interactions yield linewidths of about 2 to 5 kHz in maximum and can therefore *not* be the origin for the observed (Λ_0) (besides, dipole interactions are anisotropic). Thus, isotropic *and* magnetic field independent linewidths that vastly exceed dipolar couplings prove an enhanced internuclear coupling (*J*-coupling) mediated via electronic states. For comparison, the Λ_0 obtained from ^{77}Se in

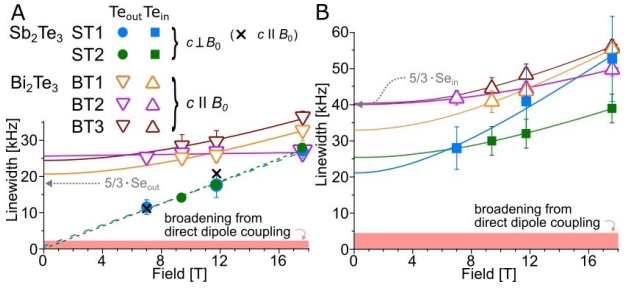

Figure 4. FWHM of Te_{out} (A) and Te_{in} (B) resonance lines for Sb_2Te_3 (circles and squares) and Bi_2Te_3 (triangles) as a function of B_0 as well as the linewidth of the single resonance for $c \parallel B_0$ (×) from ST1. Dashed and solid lines represent different field dependencies as detailed in the text. The red bars mark the expected linewidth from direct dipole-dipole interactions as obtained from the crystal structure and the method of moments.[28] Gray dotted arrows represent the field independent linewidths (Λ_0) obtained for the two Se resonances in Bi_2Se_3 after re-scaling with $^{125}\gamma/^{77}\gamma \approx 5/3$.[16]

Bi_2Se_3 are also shown in Figure 4 by the grey dotted arrows, including a re-scaling of $\times 5/3$ which accounts for the difference in the gyromagnetic ratios (γ) of ^{125}Te and ^{77}Se. The Te data from Bi_2Te_3 agree surprisingly well with the re-scaled Se linewidths in Bi_2Se_3 (for $B_0 = 0$). This suggests a similar interaction which differs chiefly due to the different hyperfine couplings of Te and Se, in good approximation relatable to the difference of their nuclear magnetic moments. Whether the coupling is of Bloembergen-Rowland (BR) type cannot readily be assessed. However, given the chemical and electronic similarities of the systems, a BR-coupling is a plausible candidate to govern also the interaction between nuclear magnetic moments in Bi_2Te_3.

In this context, the linewidths of ^{125}Te in Sb_2Te_3 are interesting. While all other resonances are affected by an enhanced internuclear coupling, Te_{out} seems not to show any field independent line broadening beyond direct dipole-dipole interactions. The smaller Λ_0 for Te_{in} in Sb_2Te_3 compared to Bi_2Te_3 may hint at a reduced interaction strength due to differences in the energy band gap as well as the nuclear spin (I) and the hyperfine coupling constants of Sb and Bi, which can be assumed to be the sole coupling partners due to the low natural abundance of ^{125}Te of about 7%. However, this consideration would not explain the absence of any enhanced linewidth of Te_{out} in Sb_2Te_3. This conundrum cannot be resolved in the present work. Note, however, that this finding is a strong argument against an RKKY-type of internuclear coupling that scales with the density of states (DOS), because Sb_2Te_3 must be assumed to have a similar, if not higher DOS than Bi_2Te_3 or Bi_2Se_3. The finding may also point to band structure details, as for example the band gap and the position of the Fermi level, which then may also be related to the topological non-trivial band inversion equally present for each of the materials under consideration. This observation may further hold key information for a better understanding of the magnetic correlations of localized moments in this type of compounds and related magnetic systems.

Conclusions

The ^{125}Te room temperature NMR of three Bi_2Te_3 and two Sb_2Te_3 single crystals is reported. In agreement with the local symmetry and the crystal structure, two Te signals are observed for both compositions. Te Spin-lattice relaxation is fast and shows large variations across the samples that cannot easily be brought into connection with the measured shift and thus hints at a special relaxation mechanism. The NMR shift anisotropy has axial symmetry, representing the trigonal symmetry of the crystal structure. Isotropic and anisotropic shift components are documented for each sample. The shift phenomenology is complex and requires further measurements including temperature dependences to allow for a deeper understanding in exchange with theory. Large, isotropic, and magnetic field independent linewidths are observed for most of the resonances in the system, proving an enhanced internuclear coupling mediated by itinerant electrons to be a ubiquitous feature of the NMR of these chalcogenides. The type of coupling mechanism could not yet be determined but may hold crucial insight for the magnetism in closely related topological insulators with localized magnetic moments.

Experimental Section

Sample preparation and characterization

The synthesis details and characterisation of the Bi_2Te_3 crystals $Bi_{1.88}Te_3$ (BT1), $Bi_{2.0}Te_3$ (BT2), and Bi_2Te_3 (BT3) have been previously reported.[14,15] Sb_2Te_3 (ST1) was synthesized using the self-flux method. Stoichiometric amounts of high purity elemental Sb and Te (both 99.999%, from *Sigma Aldrich*) were mixed inside an Ar atmosphere glovebox and loaded into a quartz tube. The ampoule was evacuated, sealed, and then heated to 730 °C. The melted precursors were kept at 730 °C for 24 hrs. The temperature of the furnace was then reduced slowly (2 K/h) to 530 °C, during which period the crystal growth took place (melting temperature of ~630 °C). The ingot obtained from the synthesis is shown in Figure 5B. Single crystals of up to a few millimeters in length and width were easily cleaved from the ingot. The other Sb_2Te_3 platelet-like crystals (ST2) were grown from a mixture of the elements slightly enriched with Te (the Sb:Te ratio 1:2). The mixture was placed in a silica ampoule, evacuated, and sealed under a dynamic vacuum ($p \leq 10^{-3}$ mbar), heated up to 580 °C at 2 C/min, kept at 580 °C for 9 days, and finally water-quenched. Several large Sb_2Te_3 crystals were mechanically separated from the ingot. Their elemental composition was determined by semi-quantitative energy dispersive X-ray analysis at 20 kV acceleration voltage on a SU8020 (Hitachi) SEM equipped with a Silicon Drift Detector (SDD) X–MaxN (Oxford). The Sb content has an average value 40.5(3) at.%, that of Te was around 59.5(4) at.%.

Powder X-ray diffraction (XRD) was performed using a *Bruker D8* diffractometer (Co-radiation) and Sb_2Te_3 powder obtained from grinding selected crystals cleaved from the center of the ingot. In Figure 5C the powder XRD pattern (top) of the Sb_2Te_3 ST1 powder and a reference pattern (ICDD reference pattern number 00-015-0874) are shown. The positions of the measured reflections and those from the reference pattern agree well with each other. No additional reflections from impurity phases were observed. Available powder XRD patterns of the Bi_2Te_3 samples (BT1 and BT2) have been reported.[15] The homogeneity of the single crystal (ST1) was

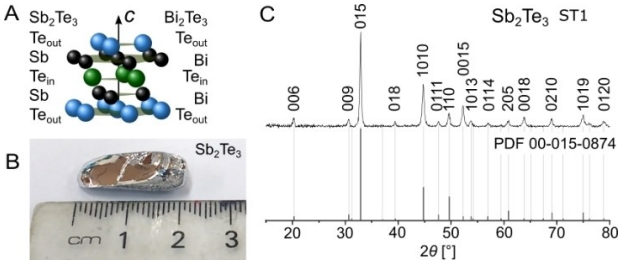

Figure 5. In panel (A), a quintuple layer (QL) of Bi_2Te_3 and Sb_2Te_3 is shown. Three QLs stacked along [001] and connected by van-der-Waals interaction built a unit cell. Te_{in} (green) and Te_{out} (blue) occupy crystallographically independent Wyckoff sites, yielding two distinct NMR signals for both samples, Te_{out} and Te_{in}. In panel (B), the Sb_2Te_3 ingot (ST1) obtained from the synthesis as described in the text is shown, and in (C), the corresponding powder XRD pattern (top) and a reference pattern (bottom) are provided.

further checked with X-ray diffraction (IPSD I diffractometer, Ag-K_α radiation), revealing, beside clear single crystal reflections, a measurable degree of mosaicity potentially related to small fragments attached to the main crystal.

NMR experiment

NMR of ^{125}Te ($\gamma/2\pi$ =13.452 MHz/T, I=1/2) was studied in magnetic fields B_0=7 T, 9.4 T, 11.7 T, and 17.4 T, with standard wide-bore NMR magnets and commercial Bruker or Techmag consoles. Small single crystals from the ingot were placed in a home-build probe equipped with a single axis goniometer to investigate angular dependences. Radio frequency coils wound around the crystal had Quality factors, Q, between 50 and 70 at room temperature. NMR spectra were recorded with a spin-echo sequence and $\pi/2$-pulse lengths ranging between 0.5 µs and 4µs. T_1 was measured using inversion-recovery or saturation-recovery pulse sequences. The NMR shift was determined with respect to $(CH_3)_2Te$ using the secondary reference method[29] and ^{63}Cu in Cu metal. The isotropic and anisotropic shift contributions, K_{iso} and K_{axial}, correspond to the resonance frequencies for $\boldsymbol{c} \parallel \boldsymbol{B}_0$ (K_{ZZ}) and $\boldsymbol{c} \perp \boldsymbol{B}_0$ (K_{XX}), as $K_{iso}=(K_{ZZ}+2K_{XX})/3$ and $K_{axial}=(K_{ZZ}-K_{XX})/3$.[23]

Acknowledgements

We thank V. Chlan (Prague), I. Garate (Sherbrooke), C. Felser (Dresden) and C. Shekhar (Dresden), as well as G. Klotzsche (Leipzig). We are grateful for the financial support by the Deutsche Forschungsgemeinschaft, Project No. 287442459148, by Leipzig University, and the MacDiarmid Institute for Advanced Materials and Nanotechnology. Open Access funding enabled and organized by Projekt DEAL.

Data Availability Statement

The data that support the findings of this study are available from the corresponding author upon reasonable request.

Conflict of Interest

The authors declare no conflict of interest.

Keywords: Topological insulators · nuclear magnetic resonance

[1] B. Poudel, Q. Hao, Y. Ma, Y. Lan, A. Minnich, B. Yu, X. Yan, D. Wang, A. Muto, D. Vashaee, X. Chen, J. Liu, M. S. Dresselhaus, G. Chen, Z. Ren, *Science* **2008**, *320*, 34–638.
[2] G. J. Snyder, E. S. Toberer, *Nat. Mater.* **2008**, *7*, 105–114.
[3] N. Xu, Y. Xu, J. Zhu, *npj Quantum Mater.* **2017**, *2*, 1–9.
[4] H. Zhang, C.-X. Liu, X.-L. Qi, X. Dai, Z. Fang, S.-C. Zhang, *Nat. Phys.* **2009**, *5*, 438–442.
[5] Y. L. Chen, J. G. Analytis, J.-H. Chu, Z. K. Liu, S.-K. Mo, X. L. Qi, H. J. Zhang, D. H. Lu, X. Dai, Z. Fang, S. C. Zhang, I. R. Fisher, Z. Hussain, Z.-X. Shen, *Science* **2009**, *325*, 178–181.
[6] Y. Ando, *J. Phys. Soc. Jpn* **2013**, *82*, 102001.
[7] D. Koumoulis, T. C. Chasapis, R. E. Taylor, M. P. Lake, D. King, N. N. Jarenwattananon, G. A. Fiete, M. G. Kanatzidis, L.-S. Bouchard, *Phys. Rev. Lett.* **2013**, *110*, 026602.
[8] D. M. Choi, C. E. Lee, *J. Korean Phys. Soc.* **2018**, *72*, 835–837.
[9] D. M. Choi, K. W. Lee, C. E. Lee, *Mater. Res. Express* **2018**, ***6***, 035019.
[10] W. Papawassiliou, A. Jaworski, A. J. Pell, J. H. Jang, Y. Kim, S.-C. Lee, H. J. Kim, Y. Alwahedi, S. Alhassan, A. Subrati, M. Fardis, M. Karagianni, N. Panopoulos, J. Dolinšek, G. Papavassiliou, *Nat. Commun.* **2020**, *11*, 1–7.
[11] M. Kotulla, U. Zülicke, *New J. Phys.* **2017**, *19*, 073025.
[12] L. Gioia, M. G. Christie, U. Zülicke, M. Governale, A. J. Sneyd, *Phys. Rev. B* **2019**, *100*, 205417.
[13] R. Guehne, V. Chlan, G. V. M. Williams, S. V. Chong, K. Kadowaki, A. Pöppl, J. Haase, *J. Magn. Reson.* **2019**, *302*, 34–42.
[14] R. Guehne, J. Haase, C. Shekhar, C. Felser, *Phys. Rev. Research* **2021**, *3*, L012018.
[15] R. Guehne, G. V. M. Williams, S. V. Chong, J. Haase, *J. Phys. Chem. C* **2021**, *125*, 6743–6748.
[16] N. M. Georgieva, D. Rybicki, R. Guehne, G. V. M. Williams, S. V. Chong, K. Kadowaki, I. Garate, J. Haase, *Phys. Rev. B* **2016**, *93*, 195120.
[17] J. Choi, S. Choi, J. Choi, Y. Park, H.-M. Park, H.-W. Lee, B.-C. Woo, S. Cho, *Phys. Status Solidi B* **2004**, *241*, 1541–1544.
[18] Y. S. Hor, P. Roushan, H. Beidenkopf, J. Seo, D. Qu, J. G. Checkelsky, L. A. Wray, D. Hsieh, Y. Xia, S.-Y. Xu, D. Qian, M. Z. Hasan, N. P. Ong, A. Yazdani, R. J. Cava, *Phys. Rev. B* **2010**, *81*, 195203.
[19] M. M. Otrokov, I. I. Klimovskikh, H. Bentmann, D. Estyunin, A. Zeugner, Z. S. Aliev, S. Gaß, A. Wolter, Koroleva, A. M. Shikin, M. Blanco-Rey, M. Hoffmann, I. R. Rusinov, A. Yu. Vyazovskaya, S. V. Eremeev, Yu. M. Koroteev, V. M. Kuznetsov, F. Freyse, J. Sánchez-Barriga, I. R. Amiraslanov, M. B. Babanly, N. T. Mamedov, N. A. Abdullayev, V. N. Zverev, A. Alfonsov, V. Kataev, B. Büchner, E. F. Schwier, S. Kumar, A. Kimura, L. Petaccia, G. Di Santo, R. C. Vidal, S. Schatz, K. Kißner, M. Ünzelmann, C. H. Min, S. Moser, T. R. F. Peixoto, F. Reinert, A. Ernst, P. M. Echenique, A. Isaeva, E. V. Chulkov, *Nature* **2019**, *76*, 416–422.
[20] N. F. Ramsey, *Phys. Rev.* **1953**, *91*, 303–307.
[21] M. A. Ruderman, C. Kittel, *Phys. Rev.* **1954**, *96*, 99–102.
[22] N. Bloembergen, T. J. Rowland, *Phys. Rev.* **1955**, *97*, 1679–1698.
[23] S. Boutin, J. Ramírez-Ruiz, I. Garate, *Phys. Rev. B* **2016**, *94*, 115204.
[24] A. O. Antonenko, E. V. Charnaya, D. Y. Nefedov, D. Y. Podorozhkin, A. V. Uskov, A. S. Bugaev, M. K. Lee, L. J. Chang, S. V. Naumov, Y A. Perevozchikova, V. V. Chistyakov, J. C. A. Huang, V. V. Marchenkov, *Phys. Solid State* **2017**, *59*, 2331–2339.
[25] R. J. Cava, H. Ji, M. K. Fuccillo, Q. D. Gibson, Y. S. Hor, *J. Mater. Chem. C* **2013**, *1*, 3176–3189.
[26] T. Harman, B. Paris, S. Miller, Goering, *J. Phys. Chem. Solids* **1957**, *2*, 181–190.
[27] J. Black, E. Conwell, L. Seigle, C. Spencer, *J. Phys. Chem. Solids* **1957**, *2*, 240–251.
[28] J. H. Van Vleck, *Phys. Rev.* **1948**, *74*, 1168–1183.
[29] R. K. Harris, E. D. Becker, S. M. C. De Menezes, P. Granger, R. E. Hoffman, K. W. Zilm, *Magn. Reson. Chem.* **2008**, *46*, 582–598.

Manuscript received: June 16, 2022
Revised manuscript received: August 31, 2022

